

This is an Open Access document downloaded from ORCA, Cardiff University's institutional repository: <https://orca.cardiff.ac.uk/id/eprint/114641/>

This is the author's version of a work that was submitted to / accepted for publication.

Citation for final published version:

Rocard, Lou, Wragg, Darren, Jobbins, Samuel A., Luciani, Lorenzo, Leoni, Stefano, Wouters, Johan and Bonifazi, Davide 2018. Templated chromophore assembly on peptide scaffolds: a structural evolution. *Chemistry - A European Journal*, -. 10.1002/chem.201803205

Publishers page: <http://dx.doi.org/10.1002/chem.201803205>

Please note:

Changes made as a result of publishing processes such as copy-editing, formatting and page numbers may not be reflected in this version. For the definitive version of this publication, please refer to the published source. You are advised to consult the publisher's version if you wish to cite this paper.

This version is being made available in accordance with publisher policies. See <http://orca.cf.ac.uk/policies.html> for usage policies. Copyright and moral rights for publications made available in ORCA are retained by the copyright holders.



Templated chromophore assembly on peptide scaffolds: a structural evolution**

Lou Rocard, Darren Wragg, Samuel Alexander Jobbins, Lorenzo Luciani,
Johan Wouters, Stefano Leoni, Davide Bonifazi*

[*] Dr. L. Rocard,^[a] D. Wragg,^[b] Dr. S. A. Jobbins,^[b] L. Luciani,^[a]
Prof. Dr. J. Wouters,^[c] Dr. S. Leoni,^[b] Prof. Dr. D. Bonifazi^[a]

^[a] Dr. L. Rocard, L. Luciani, Prof. Dr. D. Bonifazi

School of Chemistry, Cardiff University, Park Place, CF10 3AT,
Cardiff (UK)

Email: bonifazid@cardiff.ac.uk

^[b] D. Wragg, Dr. S. A. Jobbins, Dr. S. Leoni

School of Chemistry, Cardiff University, Park Place, CF10 3AT,
Cardiff (UK)

^[c] Prof. Dr. J. Wouters

Department of Chemistry, University of Namur (UNamur), 61, rue de
Bruxelles, Namur 5000 (Belgium)

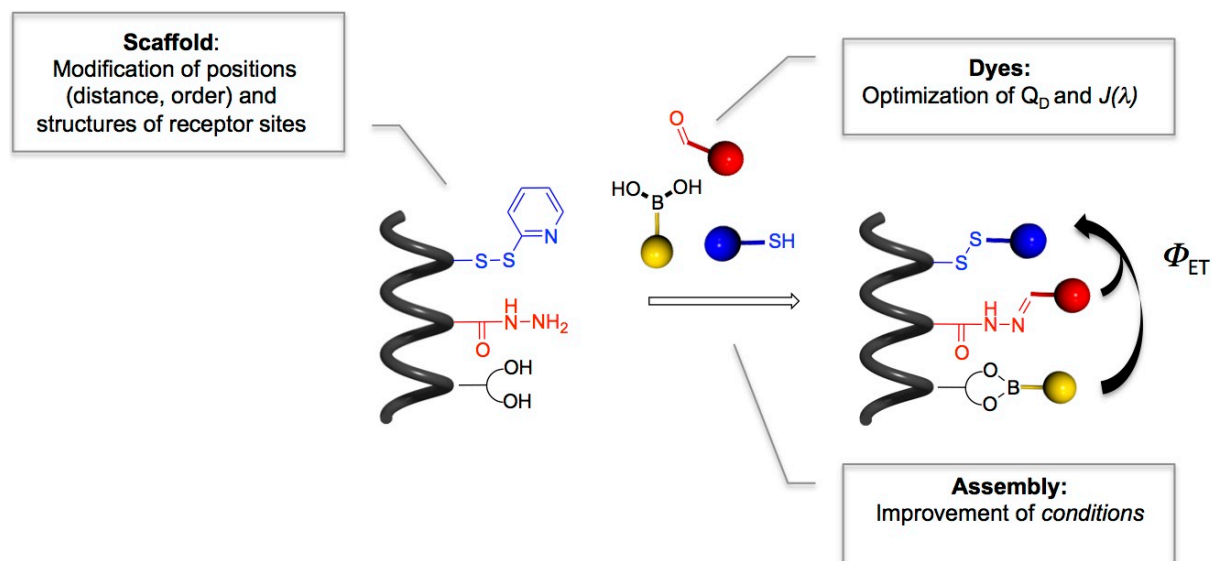
[**] DB and LR authors gratefully acknowledge the EU through the ERC
Starting Grant "COLORLANDS" and ITN-ETN "PHOTOTRAIN" projects,
and Cardiff University for the financial support.

Abstract:

The use of a template bearing pre-programmed receptor sites selectively accommodating chromophores at given positions is an attractive approach for engineering artificial light-harvesting systems. Indulging this line of thought, this work tackles the creation of tailored antenna architectures with yellow, red and blue chromophores exploiting three dynamic covalent reactions simultaneously, namely disulfide exchange, acyl hydrazone and boronic ester formations. The effect of various structural modifications, such as the chromophores as well as their spatial organization (distance, orientation, order), on the energy transfer within the antennas was studied by means of steady-state UV-Vis absorption and fluorescence spectroscopies. This systematic study allowed a significant improvement of the energy transfer efficiencies across the chromophores to a noticeable 22 and 15%, for the yellow and red donors to the blue acceptor, respectively. Metadynamics simulations suggested that the conformational properties of the antennas are driven by intramolecular chromophoric stacking interactions that, forcing the α -helix to fold on itself, annul any effects deriving from the programming of the spatial arrangement of the receptor sites in the peptide backbone.

Keywords: dynamic covalent chemistry, light-harvesting systems, energy transfer, peptide, self-assembly, metadynamics, chromophores

Figure to table of contents



Introduction

Energy is the biggest issue of the new century.^[1] Despite the very abundant and sustainable source of energy available from sunlight, nowadays only a tiny fraction of the solar energy is used by thermal collectors and solar panels to generate heat and electricity. Artificial systems usually adsorb a fraction of the solar spectrum, whereas natural photosystems can collect a much large energy fraction tailored by evolutionary selection.^[2-3] Hence, mimicking natural light-harvesting (LH) systems^[3] to efficiently capture, transfer and store energy is one of the most challenging tasks of the scientific community.^[4a-4d] In this respect, artificial antennae, with well-defined ordering of the dyes including inter-chromophoric distances, orientations and ratio donor-to-acceptor, can be developed.^[4e-4n] The supramolecular mixing of dyes,^[5] affording organogels,^[6] supramolecular polymers,^[7] co-crystals,^[8] metal-organic frameworks,^[9] is a very handy approach for engineering simple LH systems (dyads) with high donor-to-acceptor ratio. On the other hands, the covalent assembly of dyes offers a controlled route as chromophores can be assembled into robust multidimensional architectures such as multilayers,^[10] dendrimers^[11] and macrocycles,^[12] through either static or dynamic covalent linkages,^[10d, 10e, 13] allowing the efficient light collection and energy transfer control. Recently, the use of a pre-organized template (*e.g.*, proteins,^[14] nucleic acids,^[14a, 15] micelles,^[16] inorganic scaffolds^[17]) to organize distinct chromophores, has been widely explored for light harvesting. Considering its versatility, this strategy appears to be very attractive for engineering multichromophoric antennae displaying controlled spatial organization and color distribution. In a recent endeavor, we reported the creation of a multichromophoric architecture through the use of a peptidic template Ac-QLA-**X(disulfide)**-QLAQLA-**X(hydrazide)**-QLAQLA-**X(diol)**-QLA-NH₂ **1** (X = modified amino acid), in which blue naphthalene-diimide (B-NDI) **2**,^[18a] red perylene-diimide (R-PDI) **3** and yellow ethylnylpyrene (Y-Py) **4** chromophores could be spatially organized through chemoselective reactions (Figure 1).^[18b]

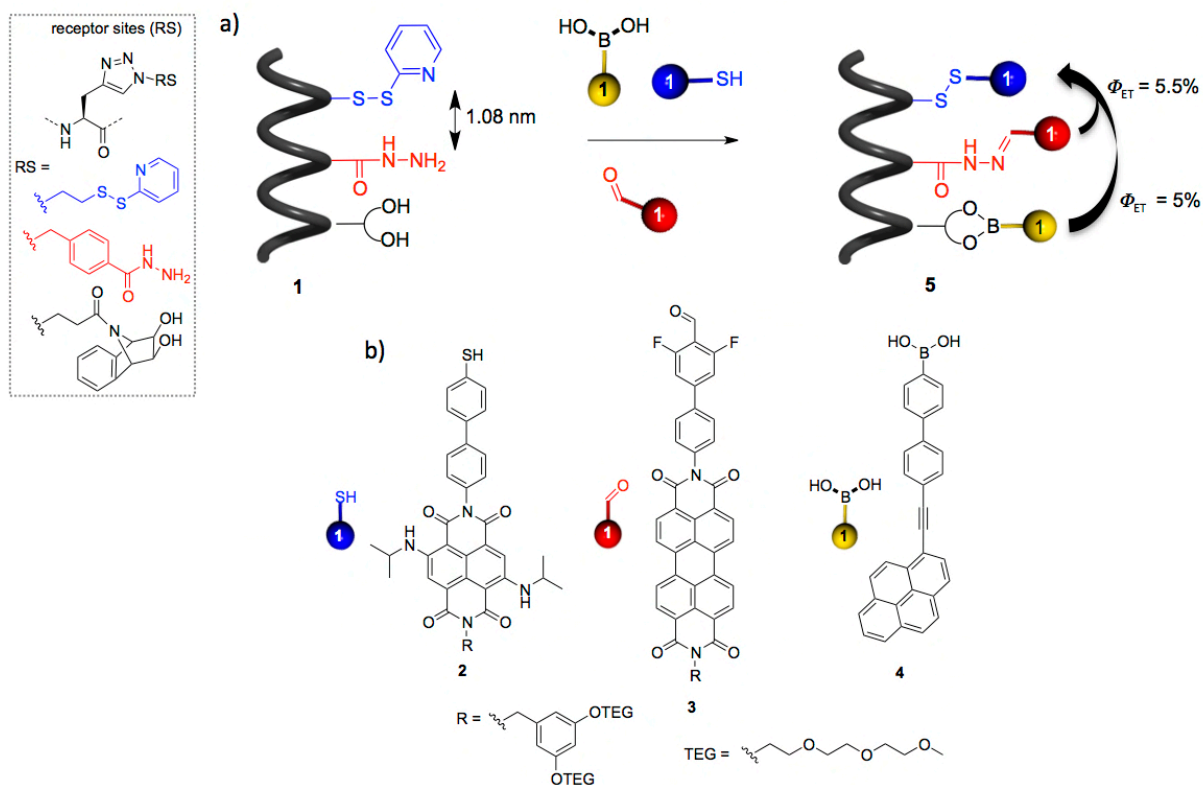


Figure 1 a) Simultaneous chromophoric assembly on pre-programmed peptide **1** (Ac-QLA-X(disulfide)-QLAQLA-X(hydrazide)-QLAQLA-X(diols)-QLA-NH₂) and energy transfer efficiencies; b) chemical structure of the first generation of dyes bearing complementary sticky side.

Specifically, the dye assembly was achieved by the simultaneous use of disulfide exchange, acyl hydrazone and boronate ester formation reactions that, taking place at tailored receptor sites on the peptidic scaffold, allowed the precise spatial programming of the chromophores. Although the proposed synthetic strategy is efficient and versatile to build multichromophoric architecture exhibiting any absorbed or emitted colors, the energy transfer efficiencies (Φ_{ET}) within triad **5**, revealed to be as low as 5% and 5.5% for the Y-Py \rightarrow B-NDI and R-PDI \rightarrow B-NDI sensitization processes, respectively (Figure 1). Thus, a structural modification of the system is required if one wants to enhance the Φ_{ET} values. Recalling Förster theory, the rate of energy transfer K_T (FRET), defined by Equation (1), depends on the interchromophoric distances r and r_0 , the latter being the critical interchromophoric distance at which the energy transfer efficiency is equal to 50%. Distance r_0 is calculated following Equation (2).^[19]

$$K_T(r) = \frac{1}{r_D} \left(\frac{r_0}{r}\right)^6 \quad (1)$$

$$r_0 = 9.78 \times 10^3 [k^2 n^{-4} Q_D J(\lambda)]^{1/6} \quad (\text{in } \text{\AA}) \quad (2)$$

Where τ_d is the fluorescent lifetime of the donor in the absence of the acceptor, k^2 described the transition dipole orientation, n is the refractive index of the medium, Q_D is the quantum yield of the donor fluorescence in the absence of the acceptor, and $J(\lambda)$ is the integral of the normalized spectral overlap between the donor emission and the acceptor absorption. Considering Q_D and $J(\lambda)$, r and k^2 as the critical variables for improving Φ_{ET} , in this work (Figure 2) we systematically studied the effect of: *i*) dyes with enhanced spectral overlap between donor emission and acceptor absorption ($J(\lambda)$) and energy-donating chromophores with high emission quantum yields (Q_D); different interchromophoric *ii*) order, *iii*) distances (r) and *iv*) orientations (variation of dipole orientation factor k^2); *v*) solvent.

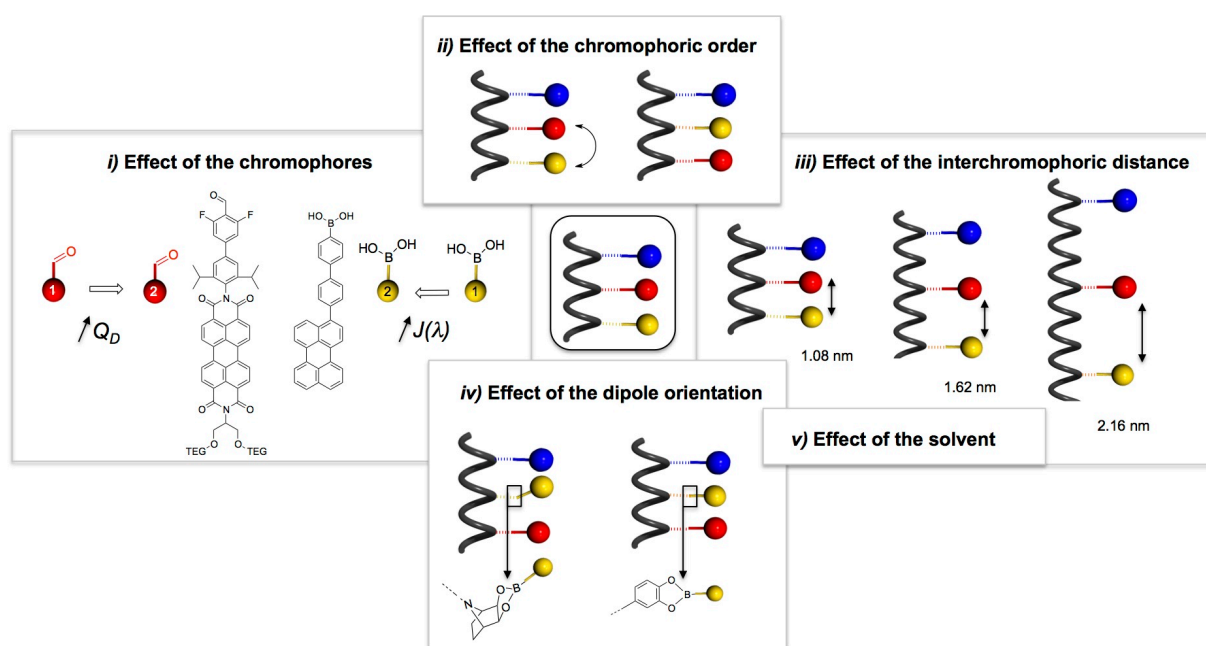


Figure 2 En route toward the structural evolution proposed in this study: *i*) effect of the chromophores; *ii*) effect of the chromophoric order; *iii*) effect of the interchromophoric distance; *iv*) effect of the dipole orientation; *v*) effect of the solvent.

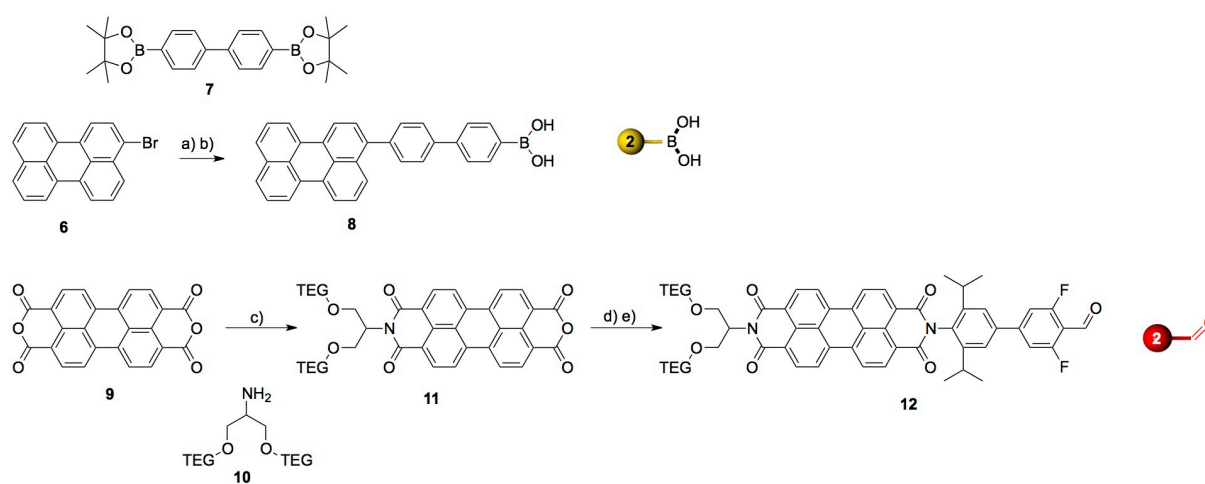
Computational simulations of all multichromophoric architectures in explicit solvent were performed to rationalize the conformational properties of the antennas. The use of molecular dynamics (MD) simulations allows for exquisite insight into the structure of the peptide and chromophores at the atomistic level, providing a means to generate and visualize the conformation of the architecture, usually

corresponding to microstates associated with a particular energy basin. However, molecular dynamics simulations are carried out on the *femtosecond* time scale, whereas the *activated processes*, such as the folding or unfolding of the peptide backbone take place over *nanosecond* or even *microsecond* timescales, meaning that unfeasibly long molecular dynamics simulations would be required before any such event can be witnessed. Besides, due to the coarse and complex nature of the underlying energy landscape of a real chemical system, the probability of transitioning from one energy basin to another is very small. Without some form of acceleration, only states separated by barriers equal to or less than thermal fluctuations ($k_B T$) in the system are likely to be visited. In order to access other regions of the configuration space, one must apply an *enhanced sampling method*, in order to facilitate the crossing of larger barriers and the observation of critical events within a reasonable time frame.^[20] One such method of acceleration, the technique used in this work, is *metadynamics*. In this technique, a history-dependent bias potential is iteratively built upon the underlying energy landscape. This discourages the system from returning to previously visited configurations and enables the systematic exploration of the configuration space. This allows for the induction and observation of structural changes, such as the folding and unfolding of the peptide backbone, which would not be possible by standard molecular dynamics simulations alone (see SI for the details).^[21]

Results and Discussions

Development of a new generation of chromophores. Following the photophysical characterization of previously engineered antenna **5**, we recognized that the emission profile of the pyrene moiety (Y-Py **4**) does not best match the UV-Vis absorption of the perylene diimide module (R-PDI **3**). Accordingly, ethynylpyrene Y-Py **4** has been substituted by a perylene chromophore (Y-Per), as the latter displays a low-energy emission profile. The optical properties of the perylene^[22] make it a suitable candidate for our architecture since it strongly absorbs in the blue region ($\epsilon = 38500 \text{ L mol}^{-1} \text{ cm}^{-1}$ at 434 nm), and is highly fluorescent with a small Stokes shift.^[23] In parallel, we also decided to amend the structure of the red chromophore, as R-PDI **3** shows a very low fluorescence quantum yield (QY) (<4%). Although

perylene bisimides and its derivatives are known to be highly fluorescent (QY >90%),^[24] electron rich benzyl N-substituents can undergo photoinduced electron transfer to the PDI core,^[24-25] thus quenching the emission of the singlet excited state. Hence, we envisaged an aliphatic linker group at the N-atom, in which the solubilizing TEG chains are attached. It is worth noting that 2,6-diisopropylphenyl substituents were also introduced to prevent parasite interchromophoric π - π stacking within the antenna.^[26] Thus, we prepared chromophores Y-Per **8** and R-PDI **12** (Scheme 1).



Scheme 1 Synthesis of Y-Per **8** and R-PDI **12**; a) **7**, K_2CO_3 , $[Pd(PPh_3)_4]$, dioxane/ H_2O , 85 °C, 3 h, 72%; b) i) $NaIO_4$, THF/ H_2O (4 :1), rt, 1 h 30, ii) HCl (1M), rt, 20 h, 90%; c) i) amine **10**, Et_3N , $iPrOH/H_2O$, 120 °C, 10 d, ii) 5% HCl (aq), 120 °C, 10 min, not isolated; d) 4-bromo-2,6-diisopropylaniline, propionic acid, MW irr, 140 °C, 7 h, 38% over two steps; e) 3,5-difluoro-4-formylphenyl boronic acid, K_2CO_3 , $[Pd(PPh_3)_4]$, dioxane/ H_2O , 80 °C, 20 h, 90%.

For the synthesis of Y-Per **8**, a Pd-catalyzed Suzuki cross-coupling was carried out between bromo-perylene **6**^[27] and 4,4'-biphenyldiboronic acid (bis)pinacol ester **7** in the presence of $[Pd(PPh_3)_4]$ and K_2CO_3 in 72% yield to afford the corresponding boronic ester. Subsequent removal of the pinacol protecting group by oxidative cleavage with $NaIO_4$ and treatment with a 1 M aqueous solution of HCl, afforded desired boronic acid Y-Per **8** in 90% yield (Scheme 1).^[28] As far as R-PDI **12** is concerned, monoanhydride intermediate **11** was obtained as a solid through mono-condensation reaction between perylene dianhydride (PDA) and amine **10**^[29] in a water/isopropanol mixture at 120 °C for ten days, a method reported by *Mattern and co.*^[30] Second condensation reaction with 4-bromo-2,6-diisopropylaniline was subsequently carried out in propionic acid at 140 °C for 7 h under microwave irradiations affording unsymmetrical PDI in 38% over two steps. Pd-catalyzed Suzuki cross-

coupling of the latter compound with 3,5-difluoro-4-formylphenyl boronic acid afforded final R-PDI **12** (Scheme 1). As expected, dyes Y-Per **8** and R-PDI **12** exhibit remarkably high QY, 70% and 94% respectively, with the emission profile of Y-Per **8** showing excellent complementary spectral properties with the absorption spectrum of R-PDI **12** (Figure 3b). Notably, the total absorption envelop of the dyes shows a good matching with the solar spectrum (Figures 3a-b).

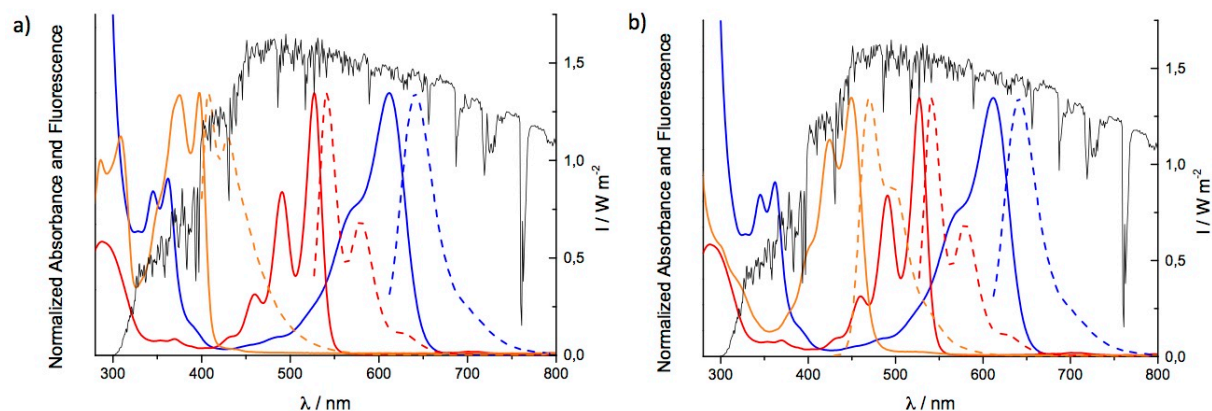


Figure 3 Normalized absorption (solid) and fluorescence (dashed) spectra of colored dyes a) 1st generation: Y-Py **4** (yellow), R-PDI **3** (red), B-NDI **2** (blue) and b) 2nd generation: Y-Per **8** (yellow), R-PDI **12** (red), B-NDI **2** (blue) in DMF plotted against the solar spectrum.

Following the self-assembly methodology previously developed by us,^[18b] the dyes were assembled on α -helix peptide **1** bearing the three-receptor sites every ($i, i+7$) residues. Multichromophoric architectures **13** and **14** were prepared with dyes *i*) Y-Per **8**, R-PDI **3**, and B-NDI **2** and with *ii*) Y-Per **8**, R-PDI **12**, and B-NDI **2**, respectively, in anhydrous DMF for 4 h in the presence of a catalytic amount of *m*-PDA and peptide **1** (Figure 4). After purification, the chemical identities of desired antennas **13** and **14** were confirmed by MALDI-TOF analyses (see SI). Antennas **13** and **14** were analyzed by UV-Vis absorption spectroscopy in DMF solution. The spectra were compared with the arithmetic sum of the three independent dyes after normalization on the B-NDI maximum at 612 nm. If characteristic bands of the three dyes were observed, a significant hypochromism for R-PDI-centered bands was also noticed, suggesting a non-quantitative introduction of the R-PDI moiety due to steric hindrance and π - π stacking interactions.

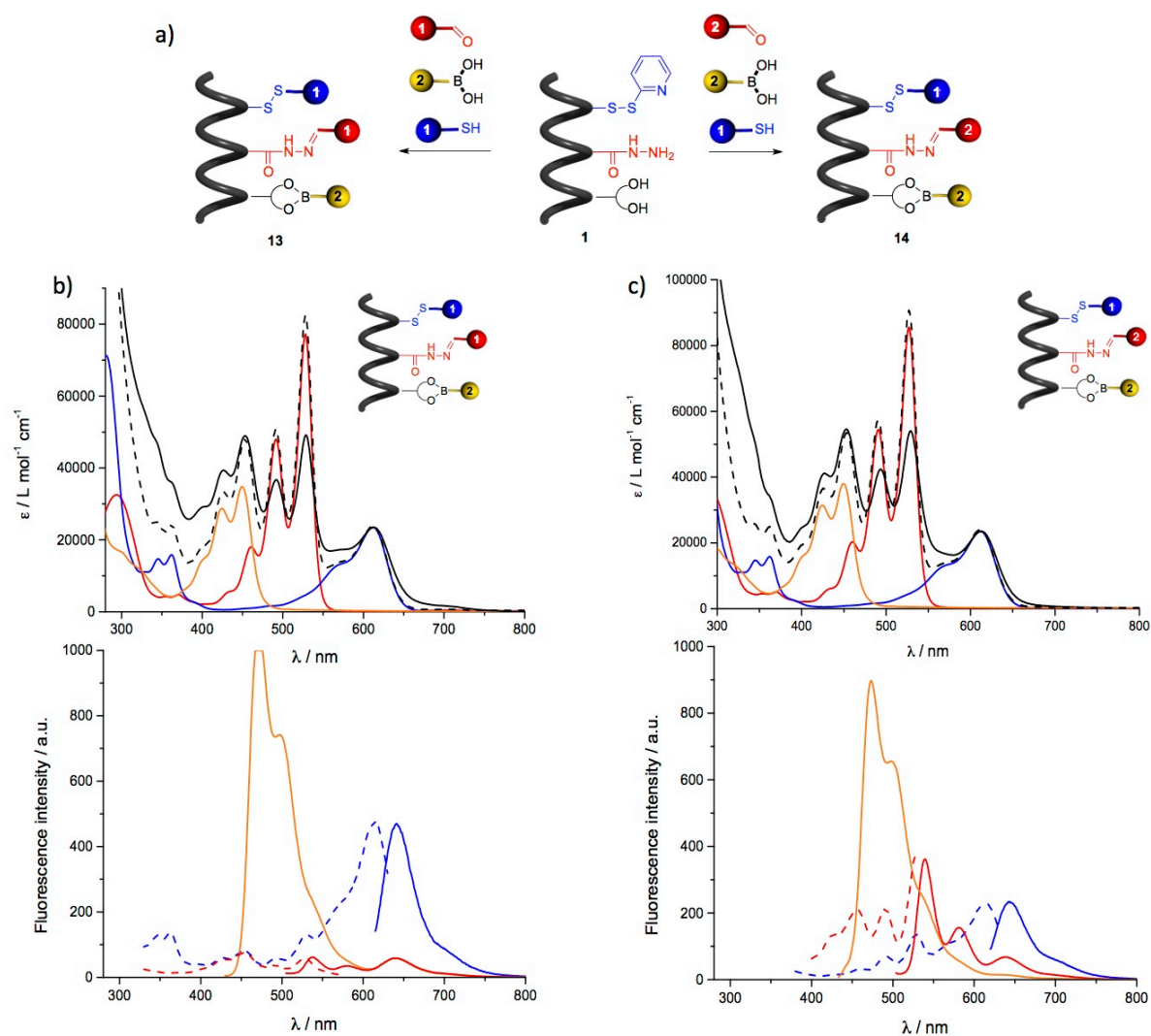


Figure 4 Colored assembly with B-NDI **2**, R-PDI **3** or **12** and Y-Per **8** on peptidic scaffold **1**; a) *m*-PDA, DMF, rt, 4 h; Middle: Absorption spectra of b) YRB peptide **13** (solid black line) and c) YRB peptide **14** (solid black line) normalized with arithmetic sum (dashed line) of absorption of dyes B-NDI **2**, R-PDI **3** or **12**, Y-Per **8** in DMF on B-NDI unit; Bottom: Emission (solid lines: $\lambda_{exc} = 423$ nm in yellow, $\lambda_{exc} = 495$ nm in red, $\lambda_{exc} = 612$ nm in blue), and corresponding normalized excitation spectra (dashed lines: $\lambda_{emis} = 540$ nm in red, $\lambda_{emis} = 640$ nm in blue) of peptides b) **13**, c) **14**.

Steady-state fluorescence measurements were performed to determine the ET efficiencies Φ_{ET} following two methods (see also SI): *Method A*) the ratio of quantum yield of acceptor B-NDI within YRB peptide (QY_{B-NDI}) is calculated upon selective excitation of the donor units R-PDI ($\lambda_{exc} = 495$ nm) or Y-Per ($\lambda_{exc} = 423$ nm) and QY_{B-NDI} upon direct excitation ($\lambda_{exc} = 609$ nm); *Method B*) the yield of energy transfer is calculated by using the equation $\Phi_{ET} = Ex_D/A_D$, where Ex_D and A_D are the fluorescence and absorption intensities of the donor in the normalized excitation and absorption spectra, respectively with the absorption and excitation spectra normalized at the maximum absorption wavelength of

blue chromophore unit B-NDI ($\lambda_{\max} = 612$ nm). For antenna **13**, $\Phi_{\text{ET}}^{(\text{Y-Per} \rightarrow \text{B-NDI})}$ and $\Phi_{\text{ET}}^{(\text{R-PDI} \rightarrow \text{B-NDI})}$ were estimated to be 7.7% and 7.7% by Method A and 7% and 7.2% with Method B, respectively. On the other hands, $\Phi_{\text{ET}}^{(\text{Y-Per} \rightarrow \text{B-NDI})}$ and $\Phi_{\text{ET}}^{(\text{R-PDI} \rightarrow \text{B-NDI})}$ values of 3.7% and 19% in antenna **14** have been measured by Method A, which revealed to be very close to those obtained by Method B (3.2% and 17.9%). A significant improvement for $\Phi_{\text{ET}}^{(\text{R-PDI} \rightarrow \text{B-NDI})}$ was observed when using R-PDI **12** from 5.5% and 7.7% for antennas **5** and **13** to 19% for architecture **14**. Metadynamics simulations of architecture **14** (Figure 5, see SI for free energy surface) show that the peptide backbone is essentially folded as α -helix, with some distortion at the nitrogen-terminal end. Notably, the PDI and NDI cores are facing to each other, while the perylene moiety hardly faces the other two chromophoric modules in any of the calculated conformations. Rather, the perylene core seems to mostly interact with the diphenyl spacers. The lack of any relevant face-to-face PDI/perylene and NDI/perylene conformations is likely to be the cause of the poor FRET between the perylene unit and the other chromophores.

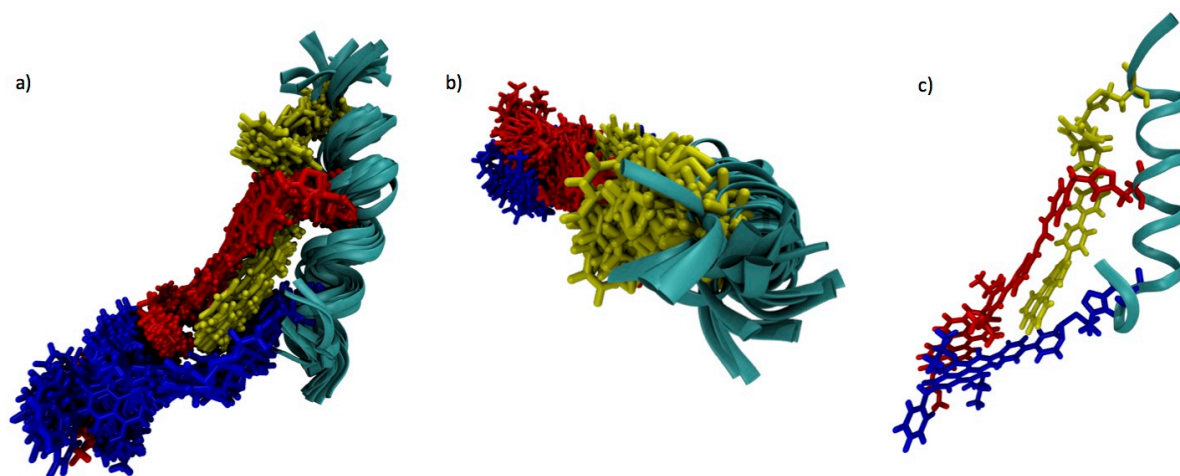


Figure 5 Metadynamics simulations of antenna **14** (100 ns); a) Side and b) top view of overlaid frames; c) most stable conformation.

Variation of the interchromophoric distance (r) and the dipole orientation. In a parallel avenue, we have investigated the effect of the interchromophoric distance. Considering that too short interchromophoric distances might prevent the quantitative linkage of the PDI moiety and favor quenching mechanisms other than energy transfers, we have decided to prepare peptide templates featuring a receptor site each ($i, i+10$) and ($i, i+14$) residues, corresponding to

three (peptide **15**) and four (peptide **16**) turns of α -helix, respectively (Figure 6). As peptide Ac-QLA-X(disulfide)-QLAQLA-X(hydrazide)-QLAQLA-X(diols)-QLA-NH₂ **1** features a receptor site each (i , $i+7$) residues with a space distance of 1.08 nm in its folded conformation, peptides **15** and **16** should lead to antenna with interchromophoric distances of 1.62 nm and 2.16 nm (pitch of α -helix = 0.54 nm), respectively.^[31] The longer interchromophoric distance might enhance the ET as it is known that maximum FRET efficiencies are observed for interchromophoric distances between 1 and 3 nm.^[32] Besides, we were also interested in studying the impact of the ordering of the chromophores on both the yield of the assembly and Φ_{ET} . In particular, we wanted to investigate the effect of the bidirectional (R-PDI \leftarrow Y-Per \rightarrow B-NDI vs. Y-Per \rightarrow R-PDI \rightarrow B-NDI) cascaded or direct energy transfers.

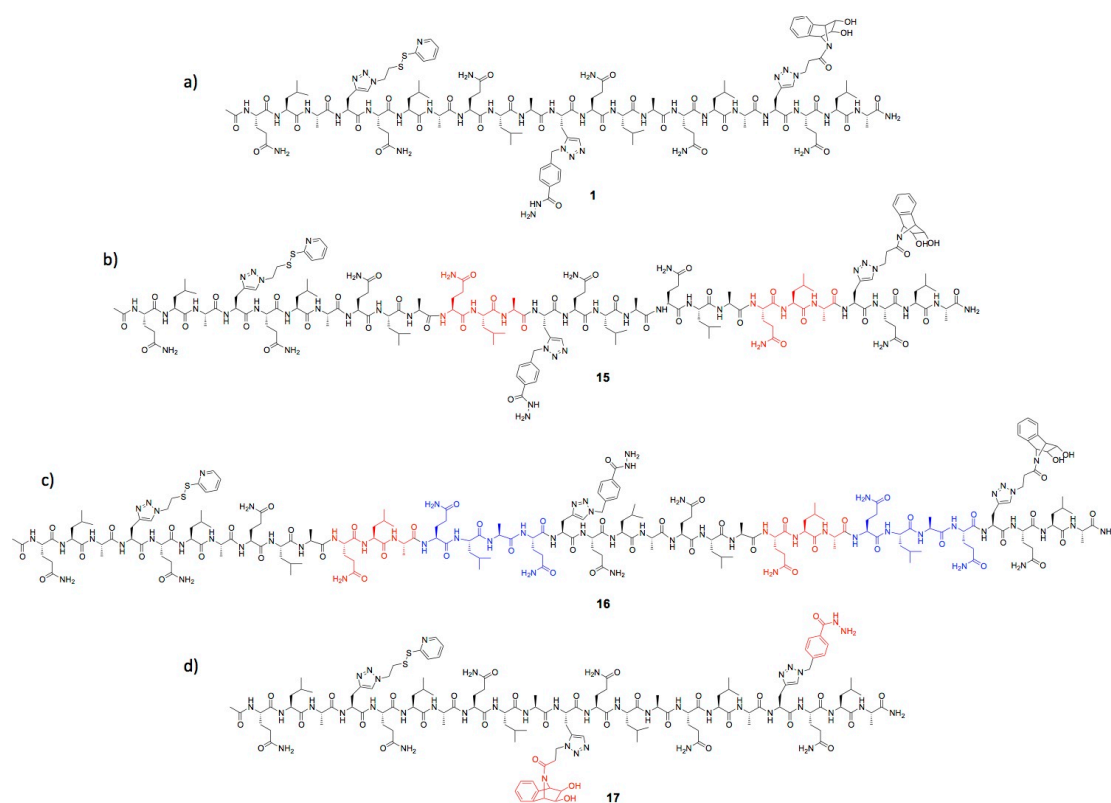
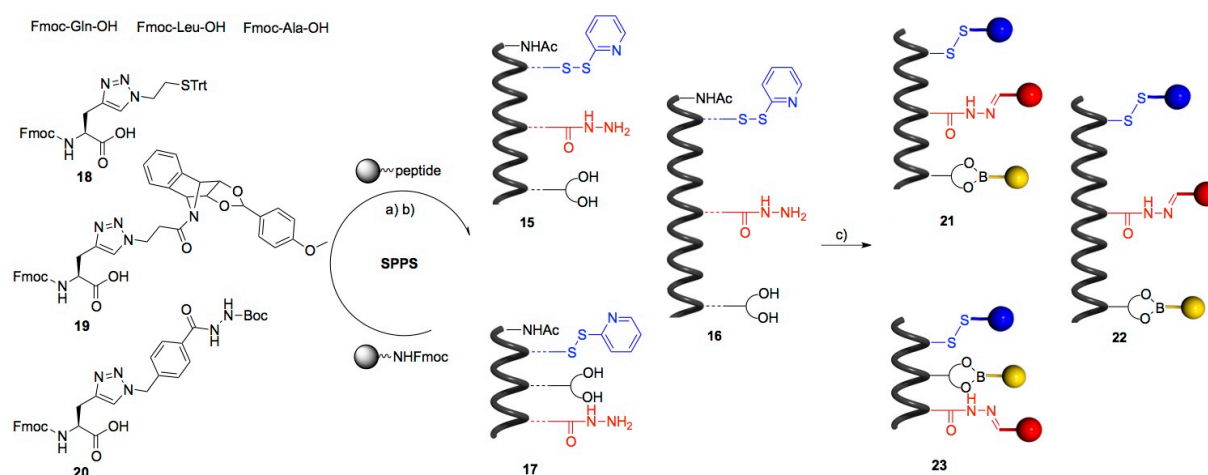


Figure 6 Structures of peptides a) **1**, b) **15**, c) **16** in which receptor sites are separated by 1.08nm, 1.62 nm and 2.16 nm, respectively; d) peptide **17** in which the order of the diol and hydrazide receptor sites is switched.

Thus, three newly designed pre-programmed peptides were synthesized (Scheme 2) by solid phase peptide syntheses (SPPS) following Fmoc/*t*Bu strategy and terminal *N*-capping: a 27-mer: Ac-QLA-X(disulfide)-QLAQLAQLA-X(hydrazide)-QLAQLAQLA-X(diols)-QLA-NH₂ **15**, a 35-mer: Ac-QLA-

X(disulfide)-QLAQLAQLAQLAQ-**X(hydrazide)**-QLAQLAQLAQLAQ-**X(diols)**-QLA-NH₂ **16** and a new 21-mer: Ac-QLA-**X(disulfide)**-QLAQLA-**X(diols)**-QLAQLA-**X(hydrazide)**-QLA-NH₂ **17**. The resin cleavage and side chain deprotection were simultaneously performed in the presence of trifluoroacetic acid (TFA)/triisopropylsilane (TIS)/H₂O/ethanedithiol (EDT) (94:1:2.5:2.5). The disulfide entities were subsequently introduced in solution by disulfide exchange with 2,2'-dipyridyl disulfide and diisopropylethylamine (DIEA) to afford the targeted peptides. After purification of the materials by RP-HPLC (see SI), the chemical identity of the peptides was confirmed by ESI-MS(Q-ToF). Simultaneous assembly of the chromophores onto peptides **15**, **16**, and **17** gave antennas **21**, **22** and **23**, respectively, following the protocol described previously (Scheme 2).^[18b] The multichromophoric architectures were purified by SEC chromatography and characterized by MALDI-TOF mass spectrometry.



Scheme 2 Synthesis of the antennas; a) SPPS: *i*) Fmoc deprotection: 20% piperidine in DMF, rt, 3 × 6 min; *ii*) AA coupling: Fmoc-AA-OH, HATU, DIEA, DMF/NMP, rt, 25 min; *iii*) Ac₂O/pyridine/NMP (1:2:2), 2 × 15 min; *iv*) TFA/TIS/H₂O/EDT (94:1:2.5:2.5), rt, 2 h; b) 2,2'-dipyridyl disulfide, DIEA, DMF, 1 h; c) Simultaneous assembly with B-NDI **2**, R-PDI **12** and Y-Per **8**, *m*-PDA, DMF, 4 h, rt.

The absorption spectra, normalized with the arithmetic sum of the absorption spectra of the three free dyes, interestingly display three different UV-vis profiles (Figure 7 Top). If a good overlapping between the two spectra was observed for antenna **23**, an hypochromism for the R-PDI-centered bands (compared to the arithmetic sum of dyes) was noticed for antennas **21** and **22**, similarly to the cases of **13** and **14**. The measured energy transfer efficiencies are gathered in Table 1. Notably, increasing the distance between the chromophores did not

significantly perturbate the Φ_{ET} values, as $\Phi_{\text{ET}}^{\text{(Y-Per} \rightarrow \text{B-NDI)}}$ was determined to be around 3% for antennas **21-22**, whereas $\Phi_{\text{ET}}^{\text{(R-PDI} \rightarrow \text{B-NDI)}}$ is 18% in the three cases. The change of the order within antenna **23** only slightly improved ET efficiencies ($\Phi_{\text{ET}}^{\text{(Y-Per} \rightarrow \text{B-NDI)}}$ and $\Phi_{\text{ET}}^{\text{(R-PDI} \rightarrow \text{B-NDI)}}$ estimated to be 7.7% and 21.9% with method A; and 7.4% and 21.8% with method B) despite the bidirectional character of the ET process.

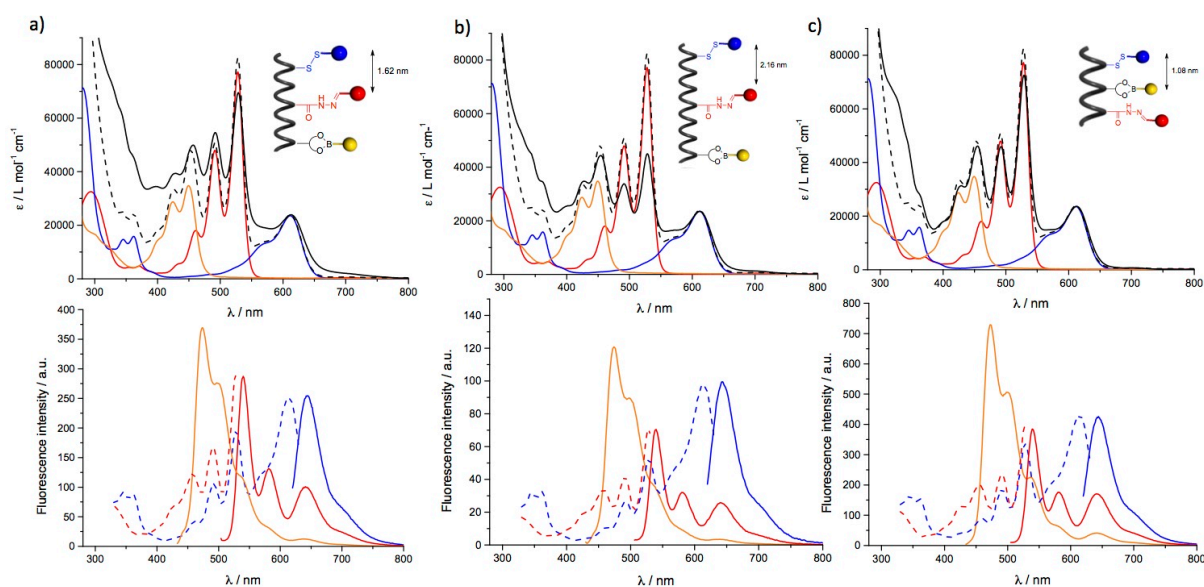


Figure 7 Top: Absorption spectra of antennas (solid black line) a) **21**, b) **22**, c) **23** normalized with the arithmetic sum of dyes (dashed black line) B-NDI **2**, R-PDI **12**, Y-Per **8** on B-NDI in DMF; Bottom: Emission (solid lines: $\lambda_{\text{exc}} = 423$ nm in yellow, $\lambda_{\text{exc}} = 495$ nm in red, $\lambda_{\text{exc}} = 612$ nm in blue), and corresponding normalized excitation spectra (dashed lines: $\lambda_{\text{emis}} = 540$ nm in red, $\lambda_{\text{emis}} = 640$ nm in blue) of antennas a) **21**, b) **22**, c) **23**.

The metadynamics calculations shown in Figure 8, clearly displayed that the energy profile is dominated by a minimum, in which the three chromophores are strongly interacting to each other in the case of antenna **21**. In contrast to antenna **14**, the perylene and NDI cores are facing to each other while the PDI core is pointing into another direction. Surprisingly, when the distance between the receptor sites was increased to 2.16 nm as in the case of **22**, the strong intramolecular stacking interaction between the different chromophores (with broader spatial occupancies) leads to a strong distortion of the helical structure of the peptidic backbone. This finding suggests that the main driving force ruling the conformation of the peptide backbone is the interchromophoric stacking and not the opposite (*i.e.*, the peptide template).

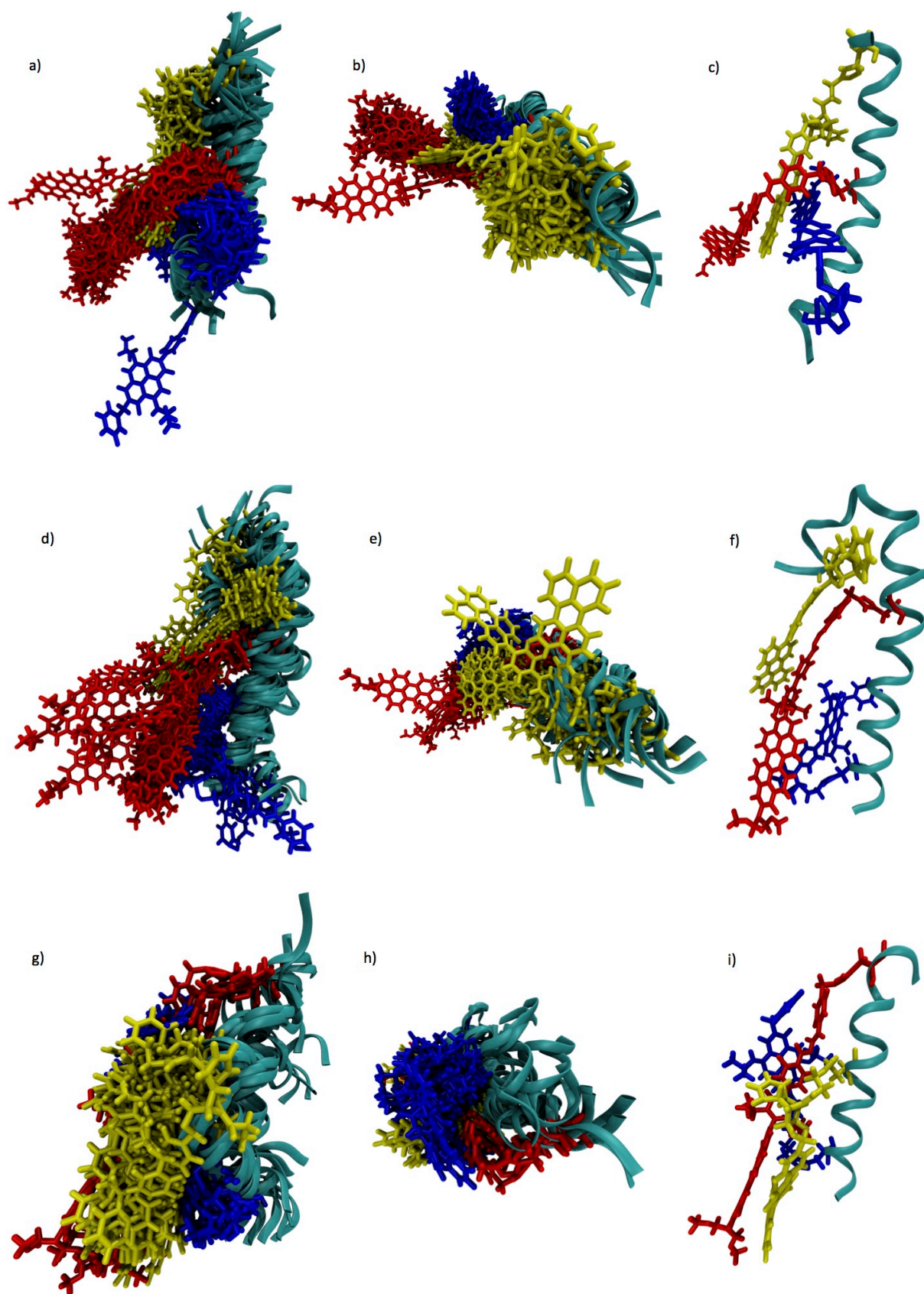


Figure 8 Metadynamics simulations (100 ns); a) d) g) side and b) e) h) top view of overlaid frames; c) f) i) most stable conformation of antennas **21**, **22**, **23** respectively.

The interchromophoric interactions annul the effect of the distances between the receptor sites in the antennas, in agreement the experimental findings for which the Φ_{ET} values are very similar for antennas **14**, **21**, and **22**. On the other hands, when the R-PDI unit is placed at terminus of the peptide (*e.g.*, antenna **23**), the deepest minimum in the energy profile corresponds to a largely α -helical structure. The folding of the flexible linker of the receptor sites led again to a strong interchromophoric stacking, in particular between the perylene and PDI cores in the case of **23**.

Replacement of the linker (orientation of the dipoles) and solvent effects. As clearly displayed in the metadynamics simulations of all antennas, the non-planar bicyclic diol anchor forces the boronic ester to adopt an unfavorable conformation for which the Y-Per core points in another direction with respect to that of chromophores R-PDI and B-NDI (Figure 5). Indeed, when looking at the crystal structures of diol-based sticky side precursors **24** and **25** (Figure 9), one can easily recognize that the diol functional group sits on a different plan than that of the linker, thus in net contrast to the directional properties of the other receptor sites. This results in an unfavorable pre-organization of the architecture preventing the chromophores to adopt face-to-face conformations. Thus, we conjectured that the non-planar bicyclic diol site could be replaced by a catechol-based linker. Thus, we investigated two catechol derivatives: one rigid, with only one sp^3 carbon between the catechol and the triazole (see amino acid precursor **26**, Scheme 3), and a second featuring three sp^3 carbons as linker (see amino acid precursor **27**, Scheme 3).

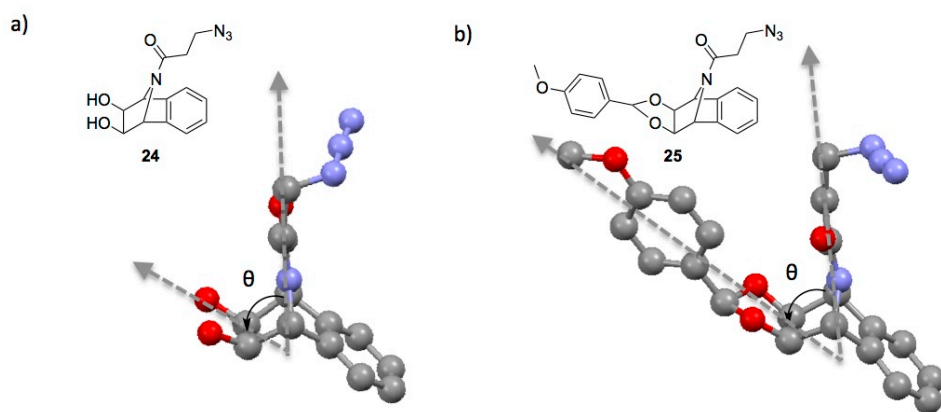
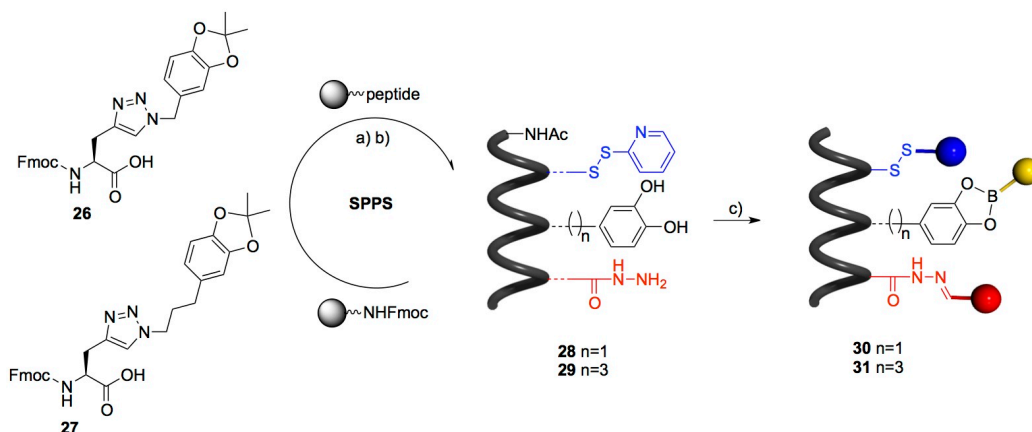


Figure 9 Side view of the crystal structures of a) diol **24** and b) protected diol **25**. Crystals were grown by slow evaporation from solutions in THF for **24** and EtOAc for **25**. Color code: grey: C, red: O and blue: N.

Accordingly, two Fmoc-protected catechol-containing amino acids **26** and **27** were synthesized (see SI) and used to prepare the peptides Ac-QLA-X(disulfide)-QLAQLA-X(catechol)-QLAQLA-X(hydrazide)-NH₂ **28** and **29** following the RYB order (Scheme 3), which so far gave the best Φ_{ET} results. After purification, the chromophore assembly was performed following the standard protocol to give antennas **30** and **31**, respectively. The absorption spectra of **30** and **31** normalized with the arithmetic sum of the absorption of the dyes on the B-NDI profile are shown in Figure 11a-b Top.



Scheme 3 Synthesis of catechol based antennas; a) SPPS: i) Fmoc deprotection: 20% piperidine in DMF, rt, 3 × 6 min; ii) AA coupling: Fmoc-AA-OH, HATU, DIEA, DMF/NMP, rt, 25 min; iii) Ac₂O/pyridine/NMP (1:2:2), 2 × 15 min; iv) TFA/TIS/H₂O/EDT (94:1:2.5:2.5), rt, 2 h; b) 2,2'-dipyridyl disulfide, DIEA, DMF, 1 h; Chromophore assembly with B-NDI **2**, R-PDI **12** and Y-Per **8**, c) *m*-PDA, DMF, 4 h, rt.

If compared to RYB peptide **23**, the measured energy transfer efficiencies for the new antennas are lower: $\Phi_{ET}^{(R-PDI \rightarrow B-NDI)}$ around 18%

and 16% for **30** and **31**, respectively; $\Phi_{ET}^{(Y-Per \rightarrow B-NDI)}$ around 4% and 5% for **30** and **31**. The metadynamics analysis for antenna **31** is depicted in Figures 10a-c. The peptide scaffold predominantly adopts an α -helical conformation, but the spatial occupancy of the dyes in antenna **31** is less confined than it is the previous antenna architectures bearing the bicyclic diol. It is worth noting that some conformations for **31** exist, in which the Y-Per unit interacts in a face-to-face fashion with the other chromophore cores (Figure 10). However, due to the large flexibility of the linkers, this strategy does seem to correctly pre-organize the dipole orientation of the dyes, and to dramatically enhance the energy transfer processes.

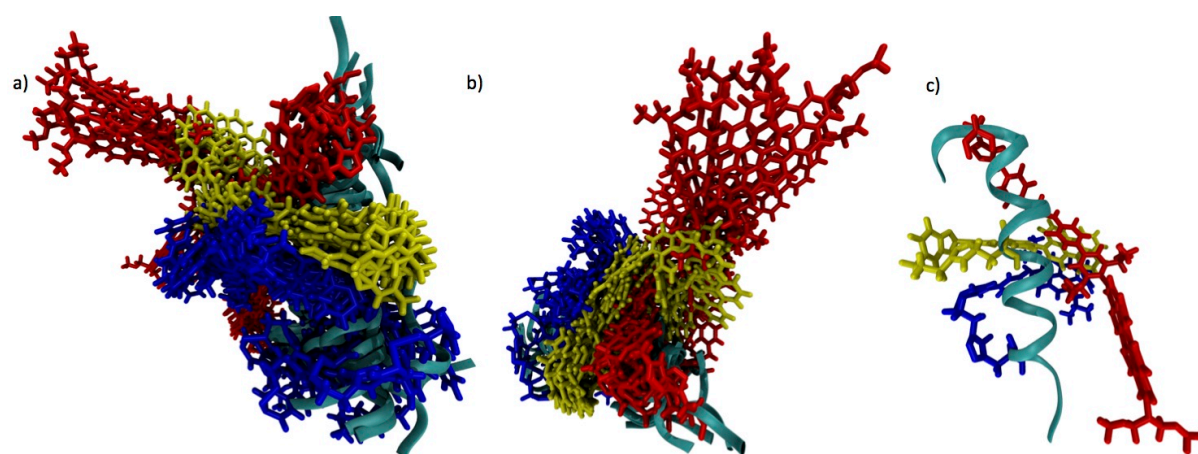


Figure 10 Metadynamics simulations of antenna **31** (100 ns); a) Side and b) top view of overlaid frames; c) most stable conformation.

Table 1 Energy transfer efficiencies.

| Entry | Peptide | Dyes Distance | Methods | $\Phi_{ET}^{(Y-Per \rightarrow B-NDI)}$ % | $\Phi_{ET}^{(R-PDI \rightarrow B-NDI)}$ % |
|-------|---------------|---------------|--|--|--|
| 1 | YRB 14 | 1.08 nm | A: $\Phi_{ET} = QY_{B-NDI}^*/QY_{B-NDI}$ | 3.7 | 17.9 |
| | | | B: $\Phi_{ET} = EX_D/A_D$ | 3.2 | 19 |
| 2 | YRB 21 | 1.62 nm | A | 2.7 | 17 |
| | | | B | 2.9 | 17 |
| 3 | YRB 22 | 2.16 nm | A | 2.5 | 19.1 |
| | | | B | 2.5 | 18.5 |
| 4 | RYB 23 | 1.08 nm | A | 7.7 | 21.9 |
| | | | B | 7.4 | 21.8 |
| 5 | | 1.08 nm | A | 4.2 | 18 |

| | | | | | |
|---|------------------------|---------|---|-----|------|
| | RYB 30 (n=1) | | B | 4 | 17.4 |
| 6 | RYB 31 (n=3) | 1.08 nm | A | 4.7 | 16.6 |
| | | | B | 4.6 | 16.2 |

On the other hand, the boronic ester linkage into catechol-based antennas **30** and **31** appears to be less stable than the one obtained from the bicyclic diol, due to the conjugation of the catechol moiety making it more Lewis acidic. Besides, we assumed that the presence of traces of Me₂N and water, coming from the thermal decomposition of DMF by the extrusion of CO, might catalyze the hydrolysis of the boronic ester linkage, especially under very diluted conditions (needed for the fluorescence measurements). The unleashing of free perylene dye in solution directly alters the $\Phi_{ET}^{(Y-Per \rightarrow B-NDI)}$ values. This consideration prompted us to consider an alternative solvent, such as dry *N,N*-dimethylacetamide (DMA). Accordingly, the assembly of the dyes was performed on Ac-QLA-X(disulfide)-QLAQLA-X(diols)-QLAQLA-X(hydrazide)-NH₂ **17** in distilled DMA to give antenna **23** after purification by SEC.

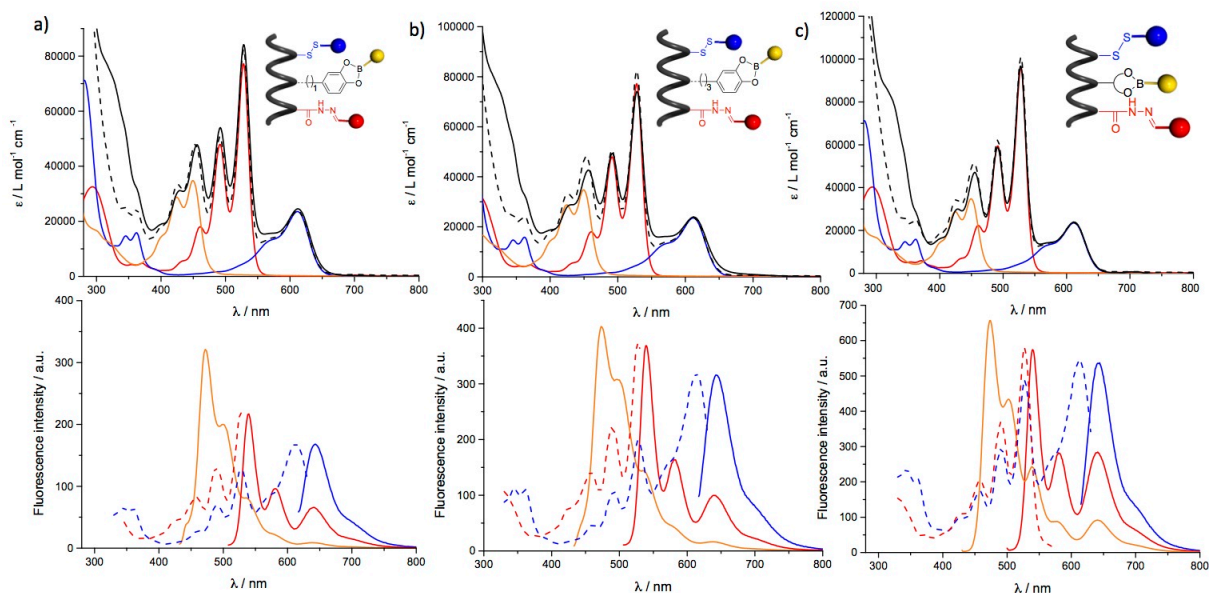


Figure 11 Top: Absorption spectra of antennas: a) RYB **30** (black solid line); b) RYB **31** (black solid line) normalized on B-NDI with arithmetic sum (dashed line) of absorption of dyes B-NDI (in blue), R-PDI (in red), Y-Per (in yellow) in DMF; c) RYB **23** (black solid line) normalized on B-NDI with arithmetic sum (dashed line) of absorption of dyes B-NDI (in blue), R-PDI (in red), Y-Per (in yellow) in DMA. Bottom: Emission (solid lines: $\lambda_{exc} = 423$ nm in yellow, $\lambda_{exc} = 495$ nm in red, $\lambda_{exc} = 609$ nm in blue), and corresponding normalized excitation spectra (dashed lines: $\lambda_{emis} = 540$ nm in red, $\lambda_{emis} = 640$ nm in blue) of antennas a) **30**, b) **31** in DMF, c) **23** in DMA.

Normalized UV-vis absorption spectrum of **23** in DMA shows a great correlation confirming the quantitative introduction of the chromophores as in the case of DMF (Figure 11c, top). Finally, the fluorescence measurements were monitored in DMA and compared with those obtained in DMF (Figure 11c, bottom). While $\Phi_{ET}^{(R-PDI \rightarrow B-NDI)}$ was estimated to be 22% in both solvents, $\Phi_{ET}^{(Y-Per \rightarrow B-NDI)}$ was determined to be around 15% (Table 2), a double value compared to that recorded in DMF. This finding further suggests that when boronic esters are used, one needs to carefully choose a suitable anhydrous solvent to avoid leakage of the chromophore in solution as consequence of parasitic hydrolysis.

Table 2 Energy transfer efficiencies within **23** in DMF and DMA.

| Entry | Peptide | Solvent | Methods | $\Phi_{ET}^{(R-PDI \rightarrow B-NDI)}$ % | $\Phi_{ET}^{(Y-Per \rightarrow B-NDI)}$ % |
|-------|---------------|---------|--|--|--|
| 1 | RYB 23 | DMF | A: $\Phi_{ET} = QY_{B-NDI}^*/QY_{B-NDI}$ | 21.9 | 7.7 |
| | | | B: $\Phi_{ET} = EX_D/A_D$ | 21.8 | 7.4 |
| 2 | RYB 23 | DMA | A | 22 | 14 |
| | | | B | 22 | 15 |

Conclusions

In conclusion, in this paper we have investigated α -helix peptides as templates to engineer antennas through a simultaneous multichromophoric assembly approach. Specifically, we systematically studied the effect of: *i*) dyes with enhanced spectral overlap between donor emission and acceptor absorption and energy-donating chromophores with high emission quantum yields; different interchromophoric *ii*) order, *iii*) distances (r) and *iv*) orientations and *v*) solvents. Replacing the ethynylpyrene chromophore with a perylene unit, with the latter displaying better spectral overlaps between donor emission and acceptor absorption as well as higher QY, revealed to have no major impact on the $\Phi_{ET}^{(Y-Per \rightarrow B-NDI)}$. However, a significant improvement of $\Phi_{ET}^{(R-PDI \rightarrow B-NDI)}$ (from 5 to ~20%) was observed with highly fluorescent PDI (QY = 94%). In a parallel avenue, we

discovered that increasing the distance between the receptor sites on the peptide scaffold (from 1.08 nm to 1.62 and 2.16 nm) did not impact the ET efficiencies as well as replacing the bicyclic diol site with a catechol derivative. Metadynamic analyses suggested that the conformations of the antennas are driven by intramolecular chromophoric stacking interactions that, forcing the α -helix to fold on itself, annul any effects deriving from the programming of the spatial arrangement of the receptor sides in the peptide backbone.

Provided that stable chromophores are used, these findings suggest that to engineer efficient antennas following a template approach one needs to select *i*) templates featuring restrained conformational properties, *ii*) highly fluorescent chromophores and *iii*) robust linkages that are chemically inert under the working conditions. It is with these guidelines that our activities will progress in the field, creeping ever closer to the ultimate goal of developing artificial antennae with unitary light-harvesting efficiency.

Additional Information

The authors declare no conflict of interest.

References

- [1] a) N. Armaroli, V. Balzani, *Chem. Eur. J.* **2016**, *22*, 32-57; b) N. Armaroli, V. Balzani, *Energy Environ. Sci.* **2011**, *4*, 3193-3222.
- [2] a) R. E. Blankenship, *Molecular Mechanisms of Photosynthesis, 2nd Edition*, Wiley-Blackwell, **2014**; b) T. Mirkovic, E. E. Ostroumov, J. M. Anna, R. Van Grondelle, Govindjee, G. D. Scholes, *Chem. Rev.* **2017**, *117*, 249-293; c) P. D. Frischmann, K. Mahata, F. Würthner, *Chem. Soc. Rev.* **2013**, *42*, 1847-1870.
- [3] a) G. D. Scholes, G. R. Fleming, A. Olaya-Castro, R. Van Grondelle, *Nat. Chem.* **2011**, *3*, 763-774; b) R. Croce, H. Van Amerongen, *Nat. Chem. Biol.* **2014**, *10*, 492-501.
- [4] a) H. Q. Peng, L. Y. Niu, Y. Z. Chen, L. Z. Wu, C. H. Tung, Q. Z. Yang, *Chem. Rev.* **2015**, *115*, 7502-7542; b) S. Kundu, A. Patra, *Chem. Rev.* **2017**, *117*, 712-757; c) A. Harriman, *Chem. Commun.* **2015**, *51*, 11745-11756; d) L. Maggini, D. Bonifazi *Chem. Soc. Rev.* **2012**, *41*, 211-241; e) A. Kremer, E. Bietlot, A. Zanelli, J. M.

- Malicka, N. Armaroli, D. Bonifazi, *Chem. Eur. J.* **2015**, *21*, 1108–1117; f) K. Yoosaf, J. Iehl, I. Nierengarten, M. Hmadeh, A. M. Albrecht-Gary, J. F. Nierengarten, N. Armaroli, *Chem. Eur. J.* **2014**, *20*, 223–231; g) V. K. Praveen, C. Ranjith, E. Bandini, A. Ajayaghosh, N. Armaroli, *Chem. Soc. Rev.* **2014**, *43*, 4222–4242; h) N. Armaroli, G. Accorsi, J. N. Clifford, J. F. Eckert, J. F. Nierengarten, *Chem. Asian J.* **2006**, *1*, 564–574; i) D. Bonifazi, G. Accorsi, N. Armaroli, F. Song, A. Palkar, L. Echegoyen, M. Scholl, P. Seiler, B. Jaun, F. Diederich *Helv. Chim. Acta* **2005**, *88*, 1839–1884; l) D. Bonifazi, M. Scholl, F. Song, L. Echegoyen, G. Accorsi, N. Armaroli, F. Diederich *Angew. Chem. Int. Ed.* **2003**, *42*, 4966–4970; m) D. Bonifazi, F. Diederich *Chem. Commun.* **2002**, *42*, 2178–2179;
- [5] S. S. Babu, D. Bonifazi, *ChemPlusChem* **2014**, *79*, 895–906.
- [6] a) A. Ajayaghosh, S. J. George, V. K. Praveen, *Angew. Chem. Int. Ed.* **2003**, *42*, 332–335; b) A. Ajayaghosh, V. K. Praveen, C. Vijayakumar, S. J. George, *Angew. Chem. Int. Ed.* **2007**, *46*, 6260–6265; c) A. Ajayaghosh, V. K. Praveen, C. Vijayakumar, *Chem. Soc. Rev.* **2008**, *37*, 109–122; d) C. Giansante, G. Raffy, C. Schafer, H. Rahma, M.-T. Kao, A. G. L. Olive, A. Del Guerzo, *J. Am. Chem. Soc.* **2011**, *133*, 316–325; e) V. K. Praveen, C. Ranjith, N. Armaroli, *Angew. Chem. Int. Ed.* **2014**, *53*, 365–368.
- [7] a) R. Abbel, C. Grenier, M. J. Pouderoijen, J. W. Stouwdam, P. E. L. G. Leclere, R. P. Sijbesma, E. W. Meijer, A. P. H. J. Schenning, *J. Am. Chem. Soc.* **2009**, *131*, 833–843; b) H. Q. Peng, J. F. Xu, Y. Z. Chen, L. Z. Wu, C. H. Tung, Q. Z. Yang, *Chem. Commun.* **2014**, *50*, 1334–1337; c) A. Liang, S. Dong, X. Zhu, F. Huang, Y. Cao, *Polym. Chem.* **2015**, *6*, 6202–6207; d) C. B. Winiger, S. Li, G. R. Kumar, S. M. Langenegger, R. Haener, *Angew. Chem. Int. Ed.* **2014**, *53*, 13609–13613; e) Y. Kubo, R. Nishiyabu, *Polymer* **2017**, *128*, 257–275.
- [8] a) P.-Z. Chen, Y.-X. Weng, L.-Y. Niu, Y.-Z. Chen, L.-Z. Wu, C.-H. Tung, Q.-Z. Yang, *Angew. Chem. Int. Ed.* **2016**, *55*, 2759–2763; b) J. Sun, A. Klechikov, C. Moise, M. Prodana, M. Enachescu, A. V. Talyzin, *Angew. Chem. Int. Ed.* **2017**, *56*, 10352–10356; c) V. Huber, S. Sengupta, F. Würthner, *Chem. Eur. J.* **2008**, *14*, 7791–7807; d) C. Röger, Y. Miloslavina, D. Brunner, A. R. Holzwarth, F. Würthner, *J. Am. Chem. Soc.* **2008**, *130*, 5929–5939.

- [9] a) C. Y. Lee, O. K. Farha, B. J. Hong, A. A. Sarjeant, S. B. T. Nguyen, J. T. Hupp, *J. Am. Chem. Soc.* **2011**, *133*, 15858–15861; b) H.-J. Son, S. Jin, S. Patwardhan, S. J. Wezenberg, N. C. Jeong, M. So, C. E. Wilmer, A. A. Sarjeant, G. C. Schatz, R. Q. Snurr, O. K. Farha, G. P. Wiederrecht, J. T. Hupp, *J. Am. Chem. Soc.* **2013**, *135*, 862–869.
- [10] a) R. S. K. Kishore, O. Kel, N. Banerji, D. Emery, G. Bollot, J. Mareda, A. Gomez-Casado, P. Jonkheijm, J. Huskens, P. Maroni, M. Borkovec, E. Vauthey, N. Sakai, S. Matile, *J. Am. Chem. Soc.* **2009**, *131*, 11106–11116; b) N. Sakai, M. Lista, O. Kel, S. I. Sakurai, D. Emery, J. Mareda, E. Vauthey, S. Matile, *J. Am. Chem. Soc.* **2011**, *133*, 15224–15227; c) G. Sforazzini, E. Orentas, A. Bolag, N. Sakai, S. Matile, *J. Am. Chem. Soc.* **2013**, *135*, 12082–12090; d) K.-D. Zhang, S. Matile, *Angew. Chem. Int. Ed.* **2015**, *54*, 8980–8983; e) K.-D. Zhang, N. Sakai, S. Matile, *Org. Biomol. Chem.* **2015**, *13*, 8687–8694.
- [11] a) M. S. Choi, T. Yamazaki, I. Yamazaki, T. Aida, *Angew. Chem. Int. Ed.* **2004**, *43*, 150–158; b) S. Hecht, J. M. J. Fréchet, *Angew. Chem. Int. Ed.* **2001**, *40*, 74–91; c) V. Balzani, G. Bergamini, P. Ceroni, E. Marchi, *New J. Chem.* **2011**, *35*, 1944–1954; d) X. Zhang, Y. Zeng, T. Yu, J. Chen, G. Yang, Y. Li, *J. Phys. Chem. Lett.* **2014**, *5*, 2340–2350; e) L. Flamigni, B. Ventura, C. C. You, C. Hippius, F. Würthner, *J. Phys. Chem. C* **2007**, *111*, 622–630.
- [12] a) R. Takahashi, Y. Kobuke, *J. Am. Chem. Soc.* **2003**, *125*, 2372–2373; b) P. Parkinson, C. E. I. Knappke, N. Kamonsutthipaijit, K. Sirithip, J. D. Matichak, H. L. Anderson, L. M. Herz, *J. Am. Chem. Soc.* **2014**, *136*, 8217–8220; c) J. Cremers, R. Haver, M. Rickhaus, J. Q. Gong, L. Favereau, M. D. Peeks, T. D. W. Claridge, L. M. Herz, H. L. Anderson, *J. Am. Chem. Soc.* **2018**, *140*, 5352–5355; d) P. Parkinson, N. Kamonsutthipaijit, H. L. Anderson, L. M. Herz, *ACS Nano* **2016**, *10*, 5933–5940; e) C. K. Yong, P. Parkinson, D. V. Kondratuk, W. H. Chen, A. Stannard, A. Summerfield, J. K. Sprafke, M. C. O'Sullivan, P. H. Beton, H. L. Anderson, L. M. Herz, *Chem. Sci.* **2015**, *6*, 181–189; f) P. Parkinson, D. V. Kondratuk, C. Menelaou, J. Q. Gong, H. L. Anderson, L. M. Herz, *J. Phys. Chem. Lett.* **2014**, *5*, 4356–4361; g) Y. Wu, R. M. Young, M. Frasconi, S. T. Schneebeli, P. Spenst,

- D. M. Gardner, K. E. Brown, F. Würthner, J. F. Stoddart, M. R. Wasielewski, *J. Am. Chem. Soc.* **2015**, *137*, 13236–13239.
- [13] a) Y. Jin, C. Yu, R. J. Denman, W. Zhang, *Chem. Soc. Rev.* **2013**, *42*, 6634–6654; b) A. Wilson, G. Gasparini, S. Matile, *Chem. Soc. Rev.* **2014**, *43*, 1948–1962; c) S. Lascano, K. D. Zhang, R. Wehlauch, K. Gademann, N. Sakai, S. Matile, *Chem. Sci.* **2016**, *7*, 4720–4724; d) H. M. Seifert, K. Ramirez Trejo, E. V. Anslyn, *J. Am. Chem. Soc.* **2016**, *138*, 10916–10924; e) B. M. Matysiak, P. Nowak, I. Cvrtila, C. G. Pappas, B. Liu, D. Komáromy, S. Otto, *J. Am. Chem. Soc.* **2017**, *139*, 6744–6751; f) J. F. Reuther, J. L. Dees, I. V. Kolesnichenko, E. T. Hernandez, D. V. Ukraintsev, R. Guduru, M. Whiteley, E. V. Anslyn, *Nat. Chem.* **2018**, *10*, 45–50.
- [14] a) C. M. Spillmann, I. L. Medintz, *J. Photochem. Photobio. C* **2015**, *23*, 1–24; b) Q. Zou, K. Liu, M. Abbas, X. Yan, *Adv. Mater.* **2016**, *28*, 1031–1043. c) F. De Leo, A. Magistrato, D. Bonifazi *Chem. Soc. Rev.* **2015**, *44*, 6916–6953.
- [15] a) Y. N. Teo, E. T. Kool, *Chem. Rev.* **2012**, *112*, 4221–4245; b) P. Ensslen, H. A. Wagenknecht, *Acc. Chem. Res.* **2015**, *48*, 2724–2733.
- [16] a) H. Q. Peng, Y. Z. Chen, Y. Zhao, Q. Z. Yang, L. Z. Wu, C. H. Tung, L. P. Zhang, Q. X. Tong, *Angew. Chem. Int. Ed.* **2012**, *51*, 2088–2092; b) W. C. Geng, Y. C. Liu, Y. Y. Wang, Z. Xu, Z. Zheng, C. B. Yang, D. S. Guo, *Chem. Commun.* **2017**, *53*, 392–395.
- [17] a) K. V. Rao, A. Jain, S. J. George, *J. Mat. Chem. C* **2014**, *2*, 3055–3064; b) Z. M. Hudson, D. J. Lunn, M. A. Winnik, I. Manners, *Nat. Commun.* **2014**, *5*, 3372.
- [18] a) A. A. Berezin, A. Sciutto, N. Demitri, D. Bonifazi, *Org. Lett.* **2015**, *17*, 1870–1873; b) L. Rocard, A. Berezin, F. De Leo, D. Bonifazi, *Angew. Chem. Int. Ed.* **2015**, *54*, 15739–15743.
- [19] a) T. Forster, *Discuss. Faraday Soc.* **1959**, *27*, 7–17; b) P. Wu, L. Brand, *Anal. Biochem.* **1994**, *218*, 1–13.
- [20] P. G. Bolhuis, D. Chandler, C. Dellago, P. L. Geissler, *Annu. Rev. Phys. Chem.* **2002**, *53*, 291–318.
- [21] A. Laio, M. Parrinello, *Proc. Natl. Acad. Sci. U. S. A.* **2002**, *99*, 12562–12566.
- [22] a) Z. Sun, Q. Ye, C. Chi, J. Wu, *Chem. Soc. Rev.* **2012**, *41*, 7857–7889; b) J. T. Markiewicz, F. Wudl, *ACS Appl. Mater. Interfaces* **2015**, *7*, 28063–28085.

- [23] I. B. Berlman, *Handbook of fluorescence spectra of aromatic molecules*, Academic Press: New York, **1971**.
- [24] F. Würthner, *Chem. Commun.* **2004**, 1564-1579.
- [25] F. Würthner, C. Thalacker, S. Diele, C. Tschierske, *Chem. Eur. J.* **2001**, 7, 2245-2253.
- [26] P. D. Frischmann, F. Würthner, *Org. Lett.* **2013**, 15, 4674-4677.
- [27] É. Torres, M. N. Berberan-Santos, M. J. Brites, *Dyes Pigm.* **2015**, 112, 298-304.
- [28] S. J. Coutts, J. Adams, D. Krolikowski, R. J. Snow, *Tetrahedron Lett.* **1994**, 35, 5109-5112.
- [29] M. R. Hansen, T. Schnitzler, W. Pisula, R. Graf, K. Muellen, H. W. Spiess, *Angew. Chem. Int. Ed.* **2009**, 48, 4621-4624.
- [30] R. Kota, R. Samudrala, D. L. Mattern, *J. Org. Chem.* **2012**, 77, 9641-9651.
- [31] N. Sewald, H. D. Jakubke, *Peptides: Chemistry and Biology: Second Edition*, Wiley-VCH, Weinheim, **2009**.
- [32] a) J. R. Lakowicz, *Principles of fluorescence spectroscopy 3rd Edition*, Springer, Singapore, **2006**; b) I. B. Berlman, *Energy Transfer Parameters of Aromatic Compounds*, Academic Press, New York, **1973**.